Phase Noise Measurements and Performance of Lasers With Non-White FM Noise for Use in Digital Coherent Optical Systems

Mustafa Al-Qadi, Maurice O'Sullivan, Chongjin Xie, and Rongqing Hui

***Abstract*—We measure the FM noise power spectral density of quantum-dot mode-locked lasers (QD-MLLs) and compare this to their measured linewidths as predictors of performance in a digital coherent system. We explain our observations in terms of the non-Lorentzian line shape of the source wherein linewidth is determined by the low frequency part of its FM noise. Investigation of system performance with simulations based on the measured phase sequences and back-to-back coherent transmission experiments show that QD-MLLs with linewidths of several megahertz can have comparable performance to that of a laser with only a few hundreds of kilohertz of Lorentzian linewidth, due to the non-white part of their FM noise. We show that spectral linewidths of lasers with similar spectral properties can underestimate their performance in coherent systems, regardless of the linewidth measurement technique used. We propose a "*Lorentzian-equivalent linewidth*" measure to characterize lasers with non-white FM noise and to estimate their impact in digital coherent optical systems. This measure is obtained from phase variations at frequencies higher than typical frequencies often used to characterize lasers with white FM noise and comparable to the system baud. The proposed measure is shown to be a better predictor of system performance than the measured linewidth, for lasers with non-white FM noise. The impact of non-white FM noise on the optimization of carrier phase recovery and system performance is also discussed.**

***Index Terms*—Coherent communication, diode lasers, mode-locked lasers, optical fiber communication.**

I. Introduction

SINCE its commercial introduction in 2008, digital coherent transmission has become a dominant technology for optical transport and datacenter interconnect (DCI). Continued progress in optical, electro-optic and application-specific integrated circuit (ASIC) technologies enable coherent transmission for short reach low power applications [1]–[4]. These are expected to include intra-DCIs, next-generation passive optical networks (NG-PONs) and modern mobile network backhaul/fronthaul systems.

Manuscript received August 19, 2019; revised November 1, 2019; accepted November 20, 2019. Date of publication November 25, 2019; date of current version March 17, 2020. This work was supported by Alibaba Group. *(Corresponding author: Mustafa Al-Qadi.)*

M. Al-Qadi and R. Hui are with the Department of Electrical Engineering and Computer Science, University of Kansas, Lawrence, KS 66045 USA (e-mail: mustafa.alqadi@ku.edu; hui@ittc.ku.edu).

M. O'Sullivan is with Ciena Corporation, Ottawa, ON K2K 0L1, Canada (e-mail: mosulliv@ciena.com).

C. Xie is with Alibaba Infrastructure Service, Alibaba Group, Sunnyvale, CA 94085 USA (e-mail: chongjin.xie@alibaba-inc.com).

Color versions of one or more of the figures in this article are available online at https://ieeexplore.ieee.org.

Digital Object Identifier 10.1109/JLT.2019.2955642

Laser phase noise can limit coherent transmission performance [5]–[8]. This noise, together with some phase noise induced by non-linear transmission, is tracked by a carrier phase recovery (CPR) circuit implemented in digital signal processing (DSP) at the receiver. The associated transmission signal-to-noise ratio (SNR) penalty is proportional to the amount of phase noise induced by the transmitter (Tx) and receiver (Rx) lasers. Laser phase noise is often characterized by a spectral linewidth, as a full-width at half-maximum (FWHM) of the power spectral density (PSD) of the unmodulated optical signal. A narrow laser linewidth, corresponding to low phase noise, can result in better system performance. Given this phase noise measure, laser linewidth $\times$ symbol period product $(\Delta v \cdot T_s)$is often used to estimate laser phase noise related system performance limit [5]–[16]. In practice, the tolerable value of $\Delta v \cdot T_s$ depends on the CPR algorithm in use, modulation format, as well as the SNR margin of the system. Based on the $\Delta v \cdot T_s$ product criterion, combined Tx and Rx laser linewidth must decrease with symbol rate to preserve CPR performance. Narrow linewidths can lead to higher laser part costs that may compromise the feasibility of the aforementioned applications at low baud. Furthermore, although coherent systems are typically required to operate at high symbol rates (e.g., 28 GBaud or higher), digital subcarrier multiplexing [1] within each wavelength channel is sometimes used to enhance system resilience to different channel impairments and this reduces the symbol rate of each subcarrier. Therefore, more in-depth investigations of the opportunities of using the currently available laser technologies in these different applications are warranted.

Distributed-feedback (DFB) lasers and external cavity lasers (ECLs) are used in communication applications. These lasers generally have white frequency modulation (FM) noise PSD, $S_{FM}(f)$, and, consequently, have a phase noise that can be suitably characterized by the FWHM, Δv, of their Lorentzian optical PSD [17]–[20]. Other types of lasers, notably quantum-dot(dash) mode-locked lasers (QD-MLLs), have a non-white FM noise PSD and, consequently, their optical PSD is not Lorentzian. QD-MLLs are multi-wavelength (comb) sources and are attractive for multi-channel applications. For these lasers, linewidth does not adequately specify the phase noise that is operative in coherent systems at different symbol rates. Thus, the $\Delta v \cdot T_s$ measure does not apply in assessing phase noise related system performance [20]. In this paper, detailed analysis about the impact of non-white FM noise in digital

coherent system performance is reported for the first time, to the authors' knowledge. This is an extended study to the observations previously reported in [20]. A blind phase search (BPS) and the *M*th-power CPR are used and compared in the system performance study. Their optimization is considered in the light of linewidth and FM noise PSD. We propose a "Lorentzian-equivalent linewidth", evaluated at relatively high measurement sampling frequencies, to estimate CPR-related penalty due to laser sources with non-Lorentzian line shape. Optical system performance is simulated by applying 16-QAM digital signal modulation on the measured waveforms of QD-MLLs' complex optical fields. The CPR algorithm performance is tested in a modeled detection to demonstrate the concept.

The rest of the paper is organized as follows. In Section II, basic theory of laser phase noise is reviewed and the relationship between FM-noise PSD and phase noise specification is discussed. Section III presents the experimental setup to extract the complex optical field of QD-MLLs and the related phase noise measurement results. System performance simulation based on the measured phase noise waveforms, optimization of CPR algorithms, and phase noise estimation efficiency are discussed in Section IV. Section V summarizes the conclusions.

II. Laser Phase Noise Characterization

A. General Characterization

For phase noise caused by spontaneous emission, phase evolution of an optical field is a random stochastic process. In the absence of intensity noise, the normalized optical field at a laser output is $E(t) = \exp\{i[\omega_0 t + \varphi(t)]\}$, where ω_0 is the optical angular (carrier) frequency and $\varphi(t)$ is the phase noise. Typically, the phase noise is constrained by specifying a FWHM linewidth, Δv, of the PSD of the envelope of $E(t)$, $S(f)$. This can be measured, for example, with a delayed self-heterodyne (DSH) detection [18] or phase noise trajectory (PNT) digital methods [17], [19]. In a measurement system, when $\varphi(t)$ is sampled at a sampling period of τ, the *phase difference* between adjacent samples is

$$\Delta\varphi_\tau(t) = \varphi(t) - \varphi(t-\tau) \tag{1}$$

This phase difference is a zero-mean Gaussian process with a variance of $\sigma_\varphi^2(\tau)$, which can be used to quantify the phase noise. The corresponding FM noise is defined as

$$\Delta f(t) = \frac{\Delta\varphi_\tau(t)}{2\pi\tau}, \tag{2}$$

and the variance $\sigma_\varphi^2(\tau)$ is related to the FM noise by [17]:

$$\sigma_\varphi^2(\tau) = 4\int_0^\infty \left(\frac{\sin(\pi f\tau)}{f}\right)^2 S_{FM}(f)\ df \tag{3}$$

where $S_{FM}(f)$ is the PSD of FM noise $\Delta f(t)$.

When $\varphi(t)$ is a Wiener process with $\Delta\varphi_\tau(t)$ a zero-mean "white" Gaussian process, $S_{FM}(f)$ should also have a white profile, according to (2). In this case, the integration in (3) results in $\sigma_\varphi^2(\tau) = 2\pi^2\tilde{S}_{FM}\tau$, where $\tilde{S}_{FM}$ is a frequency-independent FM spectral density, and the PSD of $E(t)$ has a Lorentzian shape given by

$$S(f) = \frac{\Delta v}{2\pi\left[f^2 + \left(\frac{\Delta v}{2}\right)^2\right]} \tag{4}$$

where $\Delta v = \pi\tilde{S}_{FM}$ is the FWHM of the Lorentzian function [17]. Therefore, in this model Δv is linearly related to $\sigma_\varphi^2(\tau)$ for a given τ as

$$\sigma_\varphi^2(\tau) = 2\pi\Delta v\tau \tag{5}$$

It can be inferred from (5) that in this model the measurement of Δv based on $\sigma_\varphi^2(\tau)$ is independent of the parameter τ, because the variance $\sigma_\varphi^2(\tau)$ itself is linearly proportional to τ (a well-known property for a Wiener process). Thus, for white FM noise and Lorentzian optical PSD, $\Delta v \cdot \tau$ determines phase noise variance. If, on the other hand, $S_{FM}(f)$ is not white, (4) & (5) no longer apply and the variance given by (3) is no longer linear with τ. Instead, $\sigma_\varphi^2(\tau)$ at every value of τ will depend on the specific spectral profile of $S_{FM}(f)$, as will be shown next.

B. Characterization of Lasers With Non-White FM Noise

Although many DFB lasers and ECLs have white FM noise spectra, not all practical lasers for coherent detection have the same characteristics. QD-MLLs and sampled-grating distributed Bragg reflector (SGDBR) lasers are examples of semiconductor lasers with non-white FM noise PSDs [21]–[24]. These have relatively high FM noise PSDs at the low frequency region below tens of MHz. A contrasting example is the *differential* phase noise between adjacent spectral lines of a QD-MLL, whose FM noise PSD in the low frequency region (below 10 MHz) can be an order of magnitude lower than that at frequencies around 1 GHz [25]. Measurements of different FM noise PSD profiles will be presented in the following section.

With a semi-analytic model supported by experimental demonstration, it was suggested in Ref. [26], [27] that Δv can be estimated by integrating $S_{FM}(f)$ only in the low frequency region from DC up to the point of intersection between $S_{FM}(f)$ and an FM index line given by $(8\log(2)f)/\pi^2$. This line is called the *β-separation line* and is shown as a dashed line in Fig. 1(a). Similarly, another model based on the power area method was also introduced in Ref. [28], which agrees with the findings in Ref. [26]. High frequency contents of $S_{FM}(f)$ mainly contribute to the wings of $S(f)$ at frequencies higher than those used to evaluate the FWHM spectral linewidth. On the other hand, (3) indicates that the variance $\sigma_\varphi^2(\tau)$ depends on $S_{FM}(f)$ at all frequencies. Thus, two lasers with the same $\sigma_\varphi^2(\tau)$ when evaluated at the same interval τ can have different Δv if their $S_{FM}(f)$ spectra are not the same. For the impact in the coherent system performance, CPR-related penalty is more sensitive to the untracked part of the carrier phase, largely determined by the high frequency region of $S_{FM}(f)$.

We use $\sigma_\varphi^2(\tau)$ evaluated at the system symbol interval (i.e., at $\tau = T_s$) to bound coherent CPR-related penalty for lasers with non-white FM noise. The choice of symbol interval stems from the fact that CPR algorithms operate on T_s-spaced samples. However, signal to noise ratio constraints in the measurement

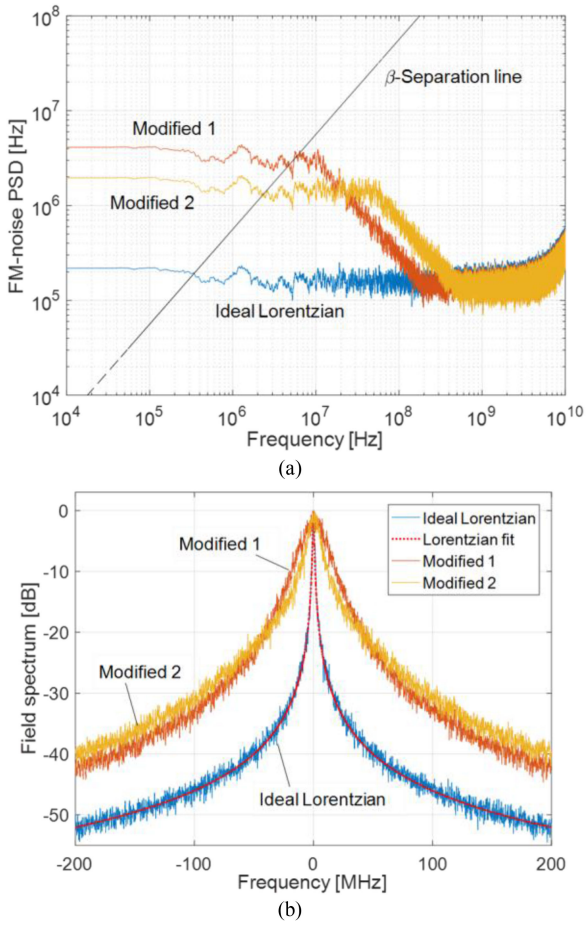

Fig. 1. (a) Simulated FM noise PSDs before (blue) and after (yellow and orange) spectral modifications and (b) corresponding optical field spectra (each normalized to its maximum PSD).

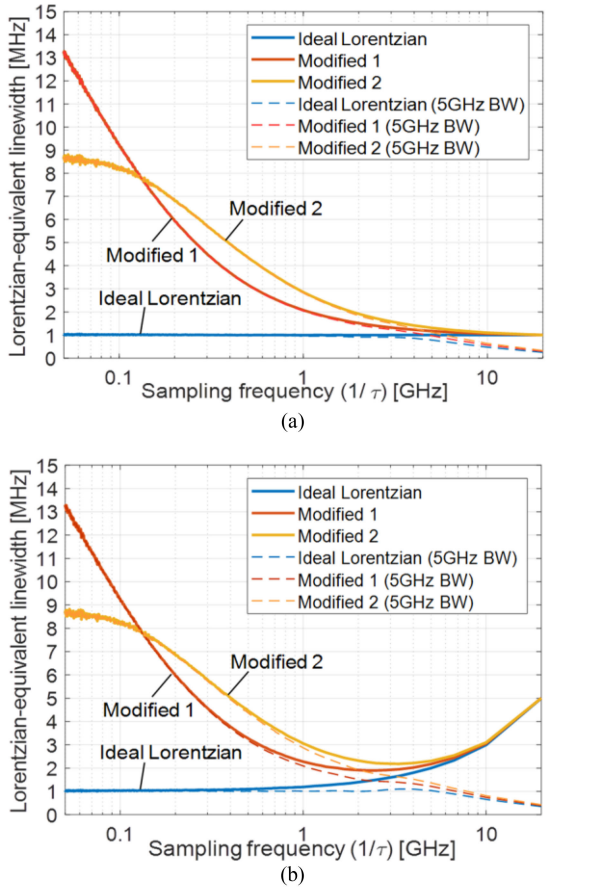

Fig. 2. Lorentzian-equivalent linewidths of the phase noise sequences used to obtain Fig. 1 (a) without and (b) with the effect of additive instrumentation noise included. BW: bandwidth.

setup may limit the feasible choice of τ to values longer than T_s in practical systems, as will be shown below. For comparison with laser sources with Lorentzian-only phase noise, the variance $\sigma_\varphi^2(\tau)$ of non-Lorentzian phase noise can be represented by a *Lorentzian-equivalent linewidth* by means of (5). We will show that, once optimized for a given non-white FM noise, the CPR algorithm performance is very close to that of a white FM noise laser with linewidth equal to the specified Lorentzian-equivalent linewidth [20].

Following this discussion, Fig. 1 shows numerically-generated phase noise with white PSD profile before (blue) and after (yellow and orange) applying spectral modifications to produce non-white FM noise. In this example, the spectral modification mask is applied to enhance the low frequency components of $S_{FM}(f)$ with a factor of G up to a specific frequency F_1. A slope of -10 dB/decade is used for the transition between the low-frequency region (up to F_1 Hz) and the high-frequency region (starts at F_2 Hz) of the spectrum. 2 million white phase noise samples were generated in the simulation at 20 GS/s with an ideal Lorentzian linewidth of 1 MHz ($\sigma_\varphi^2(\tau) = \pi \times 10^{-4}$ rad^2). Two different examples of spectral modification masks are applied with $\{F_1,\ G\} = \{10$ MHz, 20$\}$ and $\{F_1,\ G\} = \{50$ MHz, 10$\}$, labeled as "Modified 1" and "Modified 2" in Fig. 1, respectively, to represent two different lasers with non-white FM noise characteristics. The phase difference variance $\sigma_\varphi^2(\tau)$ was re-set to its original value ($\pi \times 10^{-4}$ rad^2) after applying the spectral modification. Note that since the frequency is shown in logarithmic scale, PSD reduction at high frequencies is barely noticeable. Fig. 1(b) displays the optical field PSDs corresponding to the three FM noise PSDs in Fig. 1(a), showing significant FWHM linewidth Δv enhancement due to the increase of low frequency FM noise components. With the FM noise spectral modification, Δv is increased from 1 MHz to >8 MHz despite the same value of $\sigma_\varphi^2(\tau) \cdot \Delta v$ of each spectrum in Fig. 1(b) was estimated through Lorentzian fitting, commonly used in DSH or a coherent receiver setup, by measuring the -20-dB linewidth $\Delta v_{-20\,\mathrm{dB}}$ so that $\Delta v = \Delta v_{-20\,\mathrm{dB}}/\sqrt{99}$ [29], [30].

Fig. 2(a) shows the Lorentzian-equivalent linewidths evaluated by (5) at different sampling intervals of τ. The value of τ was changed by decimating the phase sequences which were originally generated at a high sampling rate of 20 GS/s. No anti-alias filtering was used in this process because we are interested in studying the relation between $\sigma_\varphi^2(\tau)$ of the non-white FM noise

and the sampling frequency while avoiding possible measurement bandwidth limitation that would underestimate the actual phase variance [30]. Note that we will use the term "sampling frequency" hereinafter (with a unit of Hz) to represent $1/\tau$ of decimated sequences, not to be confused with the sampling rate (with a unit of Sample/s) used to generate the original phase sequences (or to acquire digital sequences in a measurement setup). As expected, the results show that for the white FM noise, the linewidth (1 MHz in this case) is obtained from phase variance through (5) independent of the sampling frequency. Thus, a low-speed digital receiver with a bandwidth of only a few hundred MHz may suffice for characterizing the phase noise through linewidth estimation [17]. On the other hand, the measured Lorentzian-equivalent linewidth can vary drastically with the change of sampling frequency for non-white FM noise. Therefore, much higher sampling frequencies are required to evaluate $\sigma_\varphi^2(\tau)$ at frequencies comparable to the symbol rate in practical coherent systems (usually $>$5 GBaud). Ideally, sampling the phase noise information at the transmission symbol rate would be desirable to measure the phase noise variance for assessing the CPR performance, which operates typically on T_s-spaced samples, as will be demonstrated in Sec. 4. However, additive noise commonly exists in the measurement setup (induced by, e.g., photodiode shot noise, and electronic circuit noise) can drastically overestimate the measured phase noise variance if wide measurement bandwidths are used [30]. Thus, limiting the measurement bandwidth is also required to reduce the impact of instrumentation noise. Nevertheless, Fig. 2(a) shows that even with non-white FM noise, the Lorentzian-equivalent linewidths evaluated at 5 GHz sampling frequency can be reasonably accurate to represent high frequency $\sigma_\varphi^2(\tau)$. In fact, limiting the signal bandwidth to 5 GHz ($\pm$2.5 GHz) affected the measurement of the Lorentzian-equivalent linewidth only marginally at the sampling frequency ($1/\tau$) of 5 GHz. Fig. 2(b) shows the effect of additive noise on the measurement with and without applying the 5 GHz bandwidth limitation. In the simulation, before extracting the signal phase, instrumentation noise was added to the unity power signal optical field with a white Gaussian PSD of -68 dB/Hz for the real and imaginary parts; resulting in a total SNR of 35 dB over a 10 GHz bandwidth. Even with this high SNR the Lorentzian-equivalent linewidths at 20 GHz were overestimated by approximately 400%. Limiting the measurement bandwidth to 5 GHz resulted in more accurate estimation of the Lorentzian-equivalent linewidth at the 5 GHz sampling frequency for all three examples of FM noise used in this simulation, with only $\sim$23% of average overestimation. In practice, the optimum measurement bandwidth will depend on the level of the additive noise and the specific phase noise characteristics of the laser. However, the examples here suggest that a sampling frequency of 5 GHz is sufficient in setups used to measure the Lorentzian-equivalent linewidths for lasers of similar non-white FM noise profiles with the wide range of $\{F_1, G\}$ parameters used for the examples shown in Fig. 1. This also dictates that a digital receiver with a sampling rate of at least 5 GS/s is required for the characterization purpose.

III. Experimental Setup and Laser Phase Noise Measurements

A number of lasers with different measured FM noise PSDs were used in this experimental study. These include: an ECL; a DFB laser; and two single-section InAs/InP QD-MLLs with different repetition frequencies. QD-MLLs are mode-locked laser sources that produce multiple spectral lines with equal spacing over a wide range of wavelengths [21], [31]. Their application has been demonstrated in multiple-lane and WDM systems [32]–[35]. Both QD-MLLs used in this work operate in the C-band with 11-GHz and 25-GHz frequency spacing between adjacent spectral lines, hereinafter denoted by "11G-MLL" and "25 G-MLL", respectively. A phase-diversity coherent receiver, comprising a 2×4 optical hybrid, two balanced photodetectors and transimpedance amplifiers, was used to down-shift the complex field envelope of the optical signal to the RF domain through heterodyne detection [17], [19], as shown in Fig. 3. The local oscillator (LO) is a tunable ECL with $<$50-kHz linewidth. A 1-nm tunable optical bandpass filter was used to select only a few spectral lines when measuring QD-MLLs. This was followed by a polarization controller to maximize the mixing efficiency between the laser under test (LUT) and the LO. A dual-channel real-time sampling oscilloscope (RTSO) operating at 50 GS/s with 23-GHz RF bandwidth was used to capture the in-phase (I) and the quadrature-phase (Q) components of the RF beat tone. Multiple sets of data, each of 10^6 samples, were recorded from each LUT over 20 μs of measurement time. Offline PC processing in MATLAB was used for phase noise analysis and CPR performance estimation [17].

To process the signal, the intermediate frequency (IF) of each captured RF waveform was shifted to the origin and the bandwidth of the heterodyne complex beat tone was then limited by a 5 GHz ideal brick-wall filter. Signal optical phase $\varphi(t)$ was then obtained by unwrapping the phase of the trajectories of recorded sample points. Fig. 4(a) shows the $S_{FM}(f)$ profiles of the 4 lasers used in this experiment. Both the ECL and the DFB lasers have relatively flat PSD profiles. In contrast, both QD-MLLs exhibit more than an order of magnitude higher PSDs in the low-frequency region extending up to tens of MHz, compared to those at the high frequency region around 1 GHz. It is important to note that these results are a property of the QD-MLLs used in this investigation [20], [22], not to be confused with the enhancement of $S_{FM}(f)$ at low frequencies stemming from extended measurement times and reported elsewhere (e.g., Ref. [17]). Fig. 4(b) shows the Lorentzian-equivalent linewidths calculated from $\sigma_\varphi^2(\tau)$ evaluated at different sampling intervals. Here τ was changed by decimating the phase sequence $\varphi(t)$ originally captured at 50 GS/s. Due to their white FM noise, the ECL and DFB laser used in this experiment have relatively constant Lorentzian-equivalent linewidths over the entire sampling frequency range. In comparison, the Lorentzian-equivalent linewidths of QD-MLLs vary by a factor of $>$10 within the same sampling frequency range. FWHM linewidths, $\Delta\upsilon$, measured from the PSDs of the beat tones, shown in the inset of Fig. 4(b),

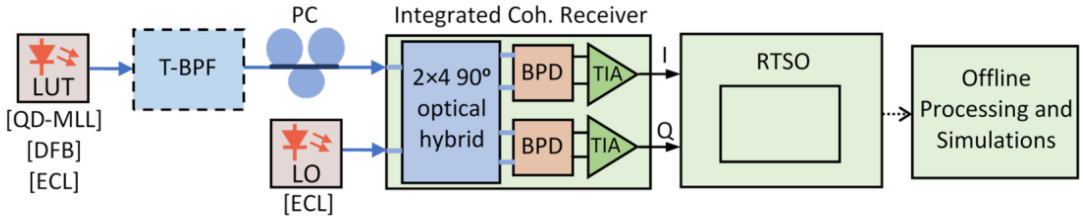

Fig. 3. Schematic of the experimental setup used for phase noise acquisition. T-BPF: tunable bandpass filter; PC: polarization control; BPD: balanced photodetector; TIA: transimpedance amplifier.

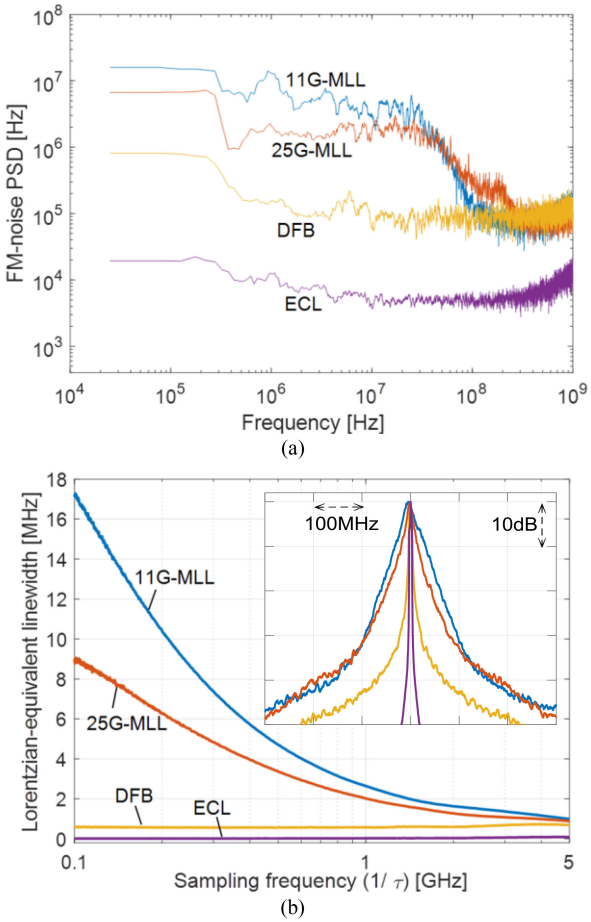

Fig. 4. (a) Experimental FM-noise PSD for different lasers. (b) Lorentzian-equivalent linewidths calculated at different sample interval τ. Inset in (b) shows the corresponding field spectra.

were comparable to the Lorentzian-equivalent linewidths calculated at the lowest sampling frequency of 0.1 GHz for all lasers. This is because low sampling frequencies are closer to the flat low-frequency region of the FM-noise PSDs (see Fig. 4(a)) for these lasers, which is closely related to the FWHM linewidths, as was explained in Sec. II B. The results in Fig. 4 illustrate the ambiguity of $\Delta\upsilon$ as a parameter to describe phase noise of lasers with non-white FM noise. Furthermore, the QD-MLLs with $\Delta\upsilon$ values of 17 MHz and 9 MHz for the 11G-MLL and the 25 G-MLL, respectively, have Lorentzian-equivalent linewidths of 1 MHz and 900 kHz near 5 GHz sampling frequency, comparable with the 700 kHz linewidth of the DFB laser. Note that if τ is equal to the symbol period T_s in a digital coherent receiver, the abscissa in Fig. 4(b) represents the symbol rate of the system. In the next section, we show that despite their relatively large FWHM linewidths, QD-MLLs exhibits similar performance as the DFB laser in coherent systems at practical symbol rates.

IV. Performance in Digital CPR Algorithms

Digital CPR algorithms can be implemented in single or multiple stages and they vary in performance and implementation complexity. For example, feed-forward CPR algorithms are practical and often used at high symbol rates [8]–[16]. These schemes typically use the blind phase search (BPS) [6] and/or the *M*th-power [10] algorithm as the main (or the only) functional stage. As such, we restrict our CPR performance evaluations to these two feed-forward methods. Without loss of generality, differential QAM encoding/decoding will be used to accommodate any quadrant jump events (or cycle slips) resulting from excess phase noise. Differential encoding induces unwanted optical SNR (OSNR) penalty overhead. However, differential encoding can be avoided only when the probability of cycle slip is very low ($\sim 10^{-18}$ < target post-FEC BER), which can be attained only in systems operating at high symbol rates and with high-quality lasers of very low phase noise [9].

In this study, measured phase sequences $\varphi(t)$ from all lasers were down-sampled by decimation to 10 GS/s and imposed on differentially-encoded 16-QAM symbols for system performance simulation. The signal-to-noise ratio per bit (E_b/N_0) was varied in the simulation by loading additive white Gaussian noise to the modulated signal before CPR and symbol-to-bit differential de-mapping. Perfect frequency offset compensation and symbol-timing recovery were asserted in the simulation to restrict the investigation to the penalty caused by residual phase noise only. A single-stage BPS with $B = 64$ test points was used [6]. The *M*th-power CPR algorithm is a constellation-partitioned 4th-power algorithm with sliding window [10]. The averaging window size was optimized in both CPR algorithms around the value of E_b/N_0 that results in BER $= 10^{-3}$ for every laser. Simulated 10 GBaud BER performance versus E_b/N_0 is shown in Fig. 5. To compare the system BER performance, ideal Lorentzian phase noises were generated numerically with the FWHM linewidths equal to the measured *Lorentzian-equivalent* linewidths of LUTs evaluated at 5 GHz (see Fig. 4(b)). At least 5 million QAM symbols were simulated and 100 bit errors were counted for each data point for BER estimation. Also shown in Fig. 5 is the simulated BER performance of ideal Lorentzian

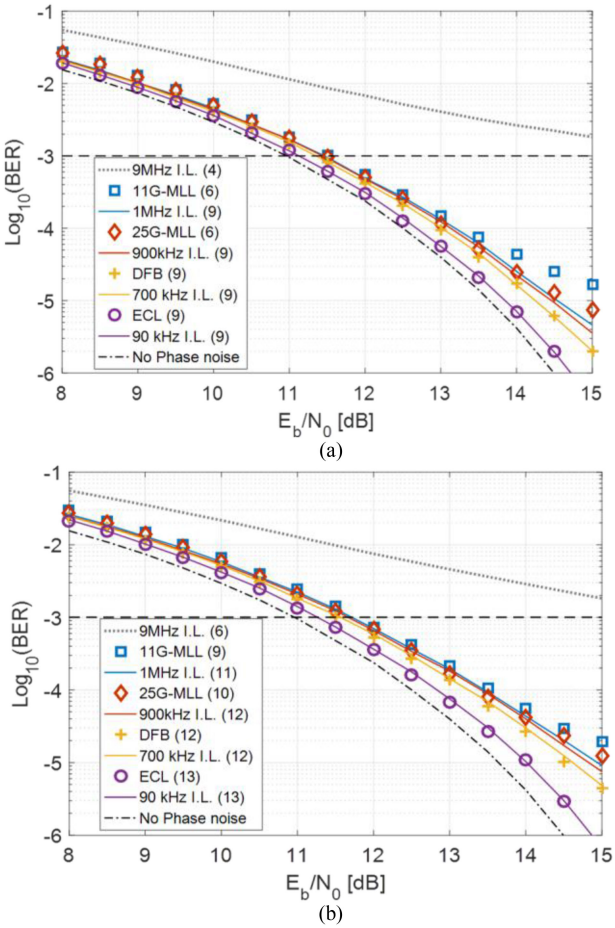

Fig. 5. Simulated BER performance for differential 16-QAM at 10 GBaud for the measured phase noises and ideal Lorentzian phase noises with (a) BPS and (b) *M*th-power CPR. Optimum half-window length used for each case is shown in the parenthetical numbers in the legends. I.L.: Ideal Lorentzian.

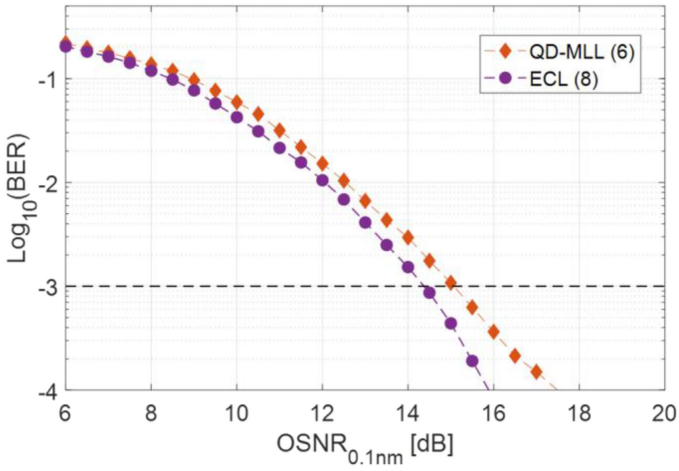

Fig. 6. Experimental B2B BER performance as a function of OSNR with differential 16-QAM at 5 GBaud for the 25 GHz-MLL and an ECL at the Tx side. BPS was used as the CPR with $B = 64$. Parenthetical numbers in the legend represent the optimum half-window length used for each case.

phase noise with the FWHM linewidth equal to the FWHM linewidth of the 25G-MLL ($\Delta v = 9$ MHz). As a reference, the dotted-dashed curve in Fig. 5 shows the BER performance in the absence of laser phase noise.

The performances of both MLLs are very close to the ideal Lorentzian phase noises with FWHM linewidths equal to the Lorentzian-equivalent linewidths of MLLs sampled at 5 GHz, except for BER floors observed at values below 10^{-5} ($<<$ typical FEC thresholds) for MLLs. For the MLLs with strong low-frequency FM noise PSDs, FWHM linewidths, mainly determined by the low-frequency components, significantly overestimate the system impact of phase noise. In fact, for a FWHM linewidth of 17 MHz, the product "$\Delta v \cdot T_s$" of this system would be 1.7×10^{-3}, which is an order of magnitude higher than a reported limit of 1.4×10^{-4} for 16-QAM for a SNR penalty of 1 dB (based on the ideal Lorentzian model) for both CPR schemes [6], [10]. Whereas system performance of the 11G-MLL with 17 MHz FWHM linewidth is comparable with the DFB laser of a FWHM of only 700 kHz. These results indicate that if FM noise is non-white, laser phase noise cannot be characterized by the FWHM linewidth, and the "$\Delta v \cdot T_s$" criterion is not adequate to assess phase-noise-induced system penalty.

To further confirm these results, we used the 25GHz-MLL in a back-to-back (B2B) coherent communication experiment and compared it to an ECL as the Tx light source. A single comb line at 1537.34 nm wavelength was used to carry a differentially encoded Nyquist 16-QAM signal at 5 GBaud with a roll-off factor of 0.1. The choice of this relatively low symbol rate was intentionally made to demonstrate the concept at an extreme condition. The output from the bandpass filter in Fig. 3, representing the selected comb line, was amplified by an Erbium-doped fiber amplifier (EDFA) and fed into an optical I/Q modulator followed by another EDFA and noise loading stage to change the OSNR of the modulated signal. The optical signal is then passed through a bandpass filter and sent to a polarization control and consequently the coherent receiver. The rest of the setup is the same as shown in Fig. 3. The I and Q components of the received signal were captured by the RTSO at a rate of 25 GS/s and processed offline. The offline receiver DSP comprised resampling to 2 Sam./sym., frequency offset compensation, root-raised cosine matched filtering, symbol timing recovery, adaptive equalization, CPR, and differential symbol-to-bit demapping for BER counting. The BPS with $B = 64$ was used for CPR. The QD-MLL was then replaced by an ECL similar to the one used as the LO (with a linewidth of $<$50 kHz) in the transmission experiment for comparison. Fig. 6 shows the BER as a function of OSNR for both the QD-MLL and the ECL as the Tx light sources. The OSNR penalty of using the QD-MLL at BER of 10^{-3} is only $\sim$0.7 dB compared to the case of the ECL. This result comes in line with the semi-numerical simulation results shown in Fig. 5. This result also demonstrates the feasibility of adopting QD-MLLs for relatively low-baud coherent applications despite their broad linewidths.

The results presented above show that for a laser with non-white FM noise, the Lorentzian-equivalent linewidth is dependent on the measurement sampling frequency, and the impact of phase noise in a coherent system is more relevant to the Lorentzian-equivalent linewidth evaluated at a relatively high

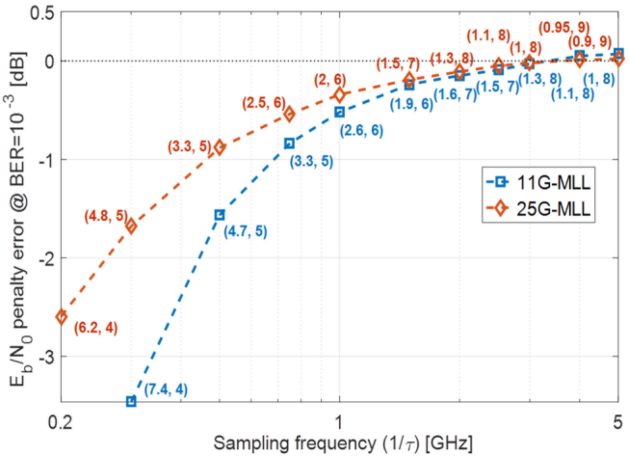

Fig. 7. Simulated E_b/N_0 penalty error between the actual performance and the Lorentzian-equivalent linewidth estimates as a function of sampling frequency. Numbers in parentheses represent the Lorentzian-equivalent linewidth in megahertz and the optimum half-window length used in the BPS CPR, respectively.

sampling frequency. Next, we investigate how the accuracy of SNR penalty estimation is affected by the choice of sampling frequency in the measurement of Lorentzian-equivalent linewidth. Fig. 7 shows the system penalty error of using Lorentzian-equivalent linewidth measured at different sampling frequencies. The system penalty error is defined as the difference of the required E_b/N_0 (to achieve BER $= 10^{-3}$) between using the actual phase noise $\varphi(t)$ of the MLLs and the numerically generated ideal Lorentzian phase noises with FWHM linewidths equal to the Lorentzian-equivalent linewidths obtained from $\varphi(t)$ decimated at different sampling frequencies. BPS was used for CPR and with optimized averaging window size for each case. The penalty errors shown in Fig. 7 diminish at relatively high sampling frequencies of higher than 3 GHz, which agrees with the results suggested by Fig. 2 for measuring Lorentzian-equivalent linewidths. Thus 5 GHz sampling frequency is generally sufficient for accurately characterizing this type of lasers for use in coherent systems. This result comes in contrast to the case of a laser with white FM noise (e.g., DFB or ECL), in which FWHM linewidth is always equal to the Lorentzian-equivalent linewidth, independent of the sampling frequency, and thus a receiver with a few hundred MHz bandwidth would be sufficient [17], [19].

A. Impact of Non-White FM Noise on Averaging Window Length

In general, all CPR algorithms in digital coherent receivers average the phase estimates over an adequate number of consecutive symbols, or window length, to reduce the effect of additive noise on the phase estimation accuracy. A longer window reduces the influence of additive noise, but also averages out instantaneous phase variations within the window and reduces the accuracy of phase estimation. Thus, window length is optimized for different phase noise and additive noise levels to achieve the best effect. It can be noted from the legends in Fig. 5 that the optimum window size is shorter for the case of non-white FM noise, compared to the ideal Lorentzian phase noise of the same Lorentzian-equivalent linewidth. To explain this effect, we consider non-white FM noise on a QPSK modulated optical signal (or, equivalently, 4-QAM), and apply the *M*th-power algorithm, in which the phase estimate at the *k*th symbol is calculated as

$$\hat{\varphi}(k) = \frac{1}{4}\arg\sum_{m=k-l}^{m=k+l}(r_m)^4 \tag{6}$$

where $r_m = d_m + n_m$ is the *m*th received complex symbol consisting of the data symbol with phase noise (d_m) and an additive zero-mean noise (n_m), and the window length is $N = 2l+1$. For a non-white FM noise with strong low-frequency components, the mean phase averaged over a certain window length will vary more compared to white FM noise scenario with equal phase variance σ_φ^2. This increased variation of averaged phase will likely require a shorter averaging time window to optimize the system performance. This can be clearly observed in the absence of additive noise. With the consideration of additive noise as a random process statistically independent of the phase noise, the total mean squared error of the phase estimate can be approximated as

$$\sigma_{err}^2(N) \cong \left\langle e_{\hat{\varphi},n}(k,N)^2\right\rangle + \left\langle e_{\hat{\varphi},pn}(k,N)^2\right\rangle \tag{7}$$

where the phase estimate total mean squared error $\sigma_{err}^2(N)$ represents the variance of the difference between the Tx-Rx combined laser phase noises and the estimated phase, i.e., $\sigma_{err}^2(N) = \mathrm{var}[\varphi(k) - \hat{\varphi}(k,N)]$, $\langle e_{\hat{\varphi},n}(k,N)^2\rangle$ is the variance of phase *estimate error* induced by the additive noise in absence of phase variations within the averaging window N, and $\langle e_{\hat{\varphi},pn}(k,N)^2\rangle$ is the variance of phase *estimate error* induced by instantaneous phase noise variations within the averaging window N in the absence of additive noise. According to (6), these quantities can be evaluated as

$$\begin{aligned}\left\langle e_{\hat{\varphi},n}(k,N)^2\right\rangle &= var\left[e_{\hat{\varphi},n}\right](N)\\ &= var\left[\frac{1}{4}arg\sum_{m=k-l}^{m=k+l}(1+n_m)^4\right]\end{aligned} \tag{8}$$

$$\begin{aligned}\left\langle e_{\hat{\varphi},pn}(k,N)^2\right\rangle &= \mathrm{var}\left[e_{\hat{\varphi},pn}\right](N)\\ &= \mathrm{var}\left[\varphi(k) - \frac{1}{4}\arg\sum_{m=k-l}^{m=k+l}e^{i4\varphi(m)}\right]\end{aligned} \tag{9}$$

We emphasize on that $\sigma_{err}^2(N)$ in (7) is only an approximation and the exact mean squared error is not a straightforward summation of the presented terms; nonetheless, it will be shown next that this is a very good approximation and it gives exact results in terms of the values of N at which minimum values of $\sigma_{err}^2(N)$ occur, which is the main focus of this analysis. The received symbols in (8) are assumed here to have a unity power and a mean phase of 0 for simplicity. However, any constant mean phase value could have been assumed without changing the results (e.g., $\pi/4$ for 4-QAM). The additive noise, n_m, is modeled as a complex Gaussian random sequence of zero mean and variance of $1/(2SNR)$ for both the real and the imaginary parts. Fig. 8 shows the numerical evaluations of (7)–(9) for

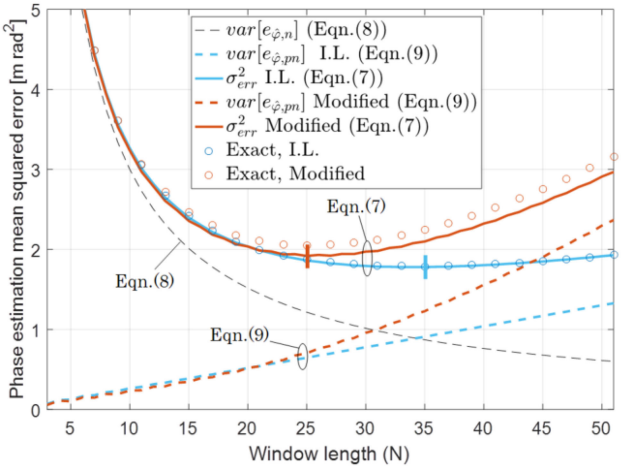

Fig. 8. Phase estimation mean squared error components for (7)–(9) evaluated over 10^5 samples for different window lengths. Vertical bars indicate points of minima on corresponding curves. I.L.: Ideal Lorentzian.

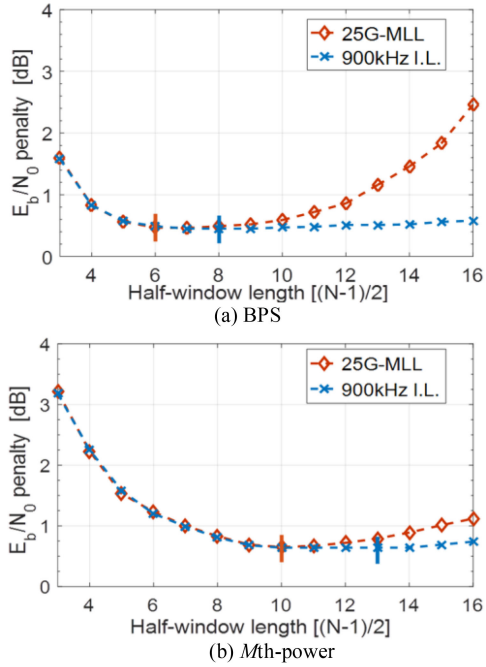

Fig. 9. E_b/N_0 penalty at BER $= 10^{-3}$ for 10 GBaud differential 16-QAM for (a) BPS and (b) Mth-power CPR. Penalties are calculated with reference to the ideal case in the absence of phase noise. Vertical bars indicate points of minima.

ideal Lorentzian phase noise with $\Delta v = 500$ kHz and non-white FM noise of the same variance generated by using the spectral modification parameters $\{F_1, G\} = \{50$ MHz, $10\}$ as was described in Sec. II B. Both phase noises have equal variance $\sigma^2_\varphi(\tau) = \pi \times 10^{-4}$ rad^2 at 10 GS/s ($\tau = 100$ ps). The *SNR* was set to 13 dB and each data point was calculated over 10^5 samples. As shown in the figure, $\mathrm{var}[e_{\hat{\varphi},pn}](N)$ increases linearly with N for ideal Lorentzian noise; but increases super-linearly for the non-white FM noise. Note that the second term on the right-hand side of (9) is equivalent to a non-weighted moving-average filter applied to the phase sequence $\varphi(k)$, known to have a linear relation between the estimate error variance and filter length when $\Delta\varphi(k) = \varphi(k) - \varphi(k-1)$ has a white Gaussian distribution [37]. The moving-average filter has low-pass characteristics with a cut-off frequency inversely proportional to the filter (window) length. This emphasizes the impact of low-frequency noise portion of $S_{FM}(f)$. As the sum of two contributions, the total mean square error σ^2_{err} in (7) has window length-dependent minima, which are demarked by vertical bars in Fig. 8. Each minimum identifies an optimum window length, which can be different for different combinations of modulation format, phase noise variance and spectral profile, and *SNR*. We observe this optimum window length contracts (from 35 to 25) for the spectrally modified phase noise due to its non-white spectral profile. The circled markers show the results of the exact values of $\sigma^2_{err}(N)$ obtained after modulating random QPSK symbols with the same phase noise sequences and *SNR* value and comparing the estimated phase noise from the *M*th-power CPR, by means of (6), to the original phase noise. They show that (7) gives very accurate results for the ideal Lorentzian case and fairly close values for the non-white FM noise case. Note that for either case the value of *N* at which the minimum σ^2_{err} occurs coincides with the prediction of (7), which shows the accuracy of the approximation made in this analysis.

This result explains the reason why the optimized window lengths are shorter for the non-white FM noise of MLLs shown in Fig. 5 (and Fig. 6) for both CPR algorithms, compared to the ideal Lorentzian phase noise of similar Lorentzian-equivalent linewidths. For the case of non-white FM noise, the phase estimation error is more sensitive to the variation of window length, and the minimum estimation error at the optimum window length is also slightly higher than that obtained with the white FM noise. This will be further discussed in the next section.

Following the analysis of optimum averaging window length, the results are confirmed by BER simulations using the measured phase noise of the 25G-MLL. Differentially encoded 16-QAM symbols were modulated on the phase sequences decimated at 10 GS/s to simulate a 10 GBaud system. Both *M*th-power and BPS based algorithms were used to obtain system penalties at BER $= 10^{-3}$ for the ideal Lorentzian phase noise and the phase noise measured from the MLL at different averaging window lengths. As shown in Fig. 9(a) & (b), the predictions obtained from the analysis above are confirmed for different CPR algorithms. The optimum window shifts to a smaller size for non-white $S_{FM}(f)$ as was predicted from Fig. 8. The increased sensitivity of system penalty to the choice of window length for non-white FM noise indicates that the CPR optimization in system design may be based on measured phase noise sequences rather than an ideal Lorentzian model.

B. Phase Estimation Efficiency and Performance Prediction Accuracy

For the case of non-white FM noise, the minimum σ^2_{err} at the optimum window length is higher than that of white FM noise as shown in Fig. 8. This can be regarded as a reduced efficiency of phase estimation, which introduces additional system SNR

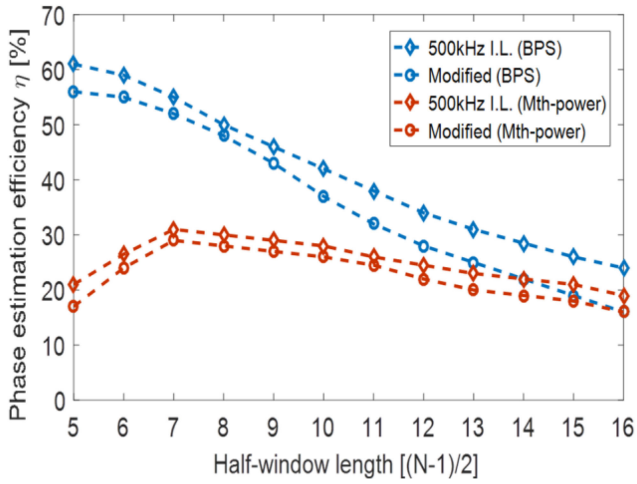

Fig. 10. Phase estimation efficiency η versus averaging window half-length for the BPS and the *M*th-power CPR for a 16-QAM signal at 10 GBaud with SNR = 17 dB.

penalty. Note that this increase of penalty was not clear in the results shown in Fig. 9(a) & (b), which we attribute to a slight overestimation of the Lorentzian-equivalent linewidth due to the instrumentation noise. In this section, the efficiency of phase estimation is studied for different $S_{FM}(f)$ profiles and CPR algorithms, and the related residual SNR penalty is quantified. CPR estimation efficiency can be measured by the ratio between the mean squared error σ_{err}^2 and the theoretical minimum achievable error expressed by the Cramér-Rao lower bound (*CRLB*) [38]. For square QAM signals with practical *SNR* values, $CRLB = 1/(2N \cdot SNR)$ [39]. The phase estimation efficiency can thus be expressed as

$$\eta(N) \equiv \frac{CRLB(N)}{\sigma_{err}^2(N)} = \frac{(2N \cdot SNR)^{-1} * 100}{\mathrm{var}\left[\varphi(k) - \hat{\varphi}(k,N)\right]} \leq 100\% \tag{10}$$

where *SNR* is the ratio between the average symbol energy and the power spectral density of additive noise, that is $E_s/N_0 = \log_2(M) \cdot E_b/N_0$.

Fig. 10 shows the calculated phase estimation efficiency versus half-window length for an ideal Lorentzian phase noise with 500 kHz linewidth and a non-white phase noise for both the *M*th-power and the BPS CPR algorithms. The non-white noise was generated with spectral modification as shown in Fig. 1(a) with parameters $\{F_1, G\} = \{50$ MHz, 10$\}$, and slope = -10 dB/decade. Both the white and the non-white phase noises have the same phase difference variance $\sigma_\varphi^2(\tau) = \pi \times 10^{-4}$ rad^2 sampled at 10 GS/s ($\tau = 100$ ps). The optical field with phase noise was loaded with 16-QAM symbols, and *SNR* was set to 17 dB through noise loading. In comparison to the *M*th-power CPR, BPS algorithm has better phase estimation efficiency, especially for short averaging windows. The phase estimation efficiency is lower for the laser with non-white FM noise compared to that with white FM noise for both CPR algorithms, and this difference is more pronounced for the BPS at long window lengths. This agrees with the fast increase of *SNR* penalty with the window length shown in Fig. 9(a) for the non-white FM noise sequences of the 25G-MLL.

Note that although system penalty due to phase noise is closely related to phase estimation efficiency, it cannot be assessed solely by this efficiency. This is because BER is also affected by the probability of cycle slips which are not included in the calculation of phase estimation efficiency, as have been removed before calculating the estimation error in the denominator of (10). The probability of cycle slip events can vary for different profiles of $S_{FM}(f)$. Therefore, for the case of non-white FM noise, it is more accurate to investigate the phase-noise-induced *SNR* penalty directly from the BER calculation after CPR.

To investigate the impact of non-white FM noise on *SNR* penalty without the ambiguity of laser characterization errors, we run a computer simulation using digitally generated phase noise sequences with increased low-frequency components in $S_{FM}(f)$ as described in Sec. II B. Ideal Lorentzian phase noise was first generated with a linewidth of 500 kHz or 1 MHz. Spectral modification was then applied to generate the non-white FM noise with $G = 10$ and 20. The parameter F_1 was swept from 0 to 300 MHz in 20 equal steps on the logarithmic frequency scale, representing different bandwidths of low-frequency excess FM noise. The phase difference variance $\sigma_\varphi^2(\tau)$ of the spectrally-modified non-white FM noise is then rescaled to its original value before spectral modification [$\sigma_\varphi^2(100\,ps) = 2\pi \times 10^{-4}$ or $\pi \times 10^{-4}$ rad^2 at 10 GS/s]. This assures that all phase noise sequences with different spectral profiles have the same Lorentzian-equivalent linewidth at $\tau = 100$ ps, although they may have very different FWHM linewidths. The results of this simulation will also show the accuracy of using Lorentzian-equivalent linewidth sampled at the signal symbol rate in predicting system performance, regardless of the actual FWHM linewidth of the laser and measurement-induced errors. Figs. 11(a) and (b) show the E_b/N_0 penalty (for BER = 10^{-3}) as the function of F_1 for the Lorentzian-equivalent linewidths of 1 MHz and 500 kHz, respectively. 16-QAM differential encoding is used to generate the 10 GBaud signal with 5 million data symbols simulated at each point. BPS is employed for CPR with $B = 64$ [6]. The optimum window length (indicated by the right y-axes in the figures) was optimized for each value of F_1. The penalty was calculated with reference to the ideal case without phase noise and was found to be 0.33 dB and 0.49 dB for the ideal Lorentzian phase noise without spectral modification, for the linewidths of 500 kHz and 1 MHz, respectively (see horizontal dashed lines in the figures). With the increased low frequency components of $S_{FM}(f)$ through spectral modification, the penalty starts to increase when the frequency F_1 reaches to a few 10s of MHz (~0.1% of symbol rate), and the optimum window length is reduced accordingly with the increase of F_1. For the case shown in Fig. 11(a), the spectral modification increases the FWHM linewidths from 500 kHz to 4 MHz and 6 MHz, with $F_1 = 100$ MHz and $G = 10$ and 20, respectively, but the system penalty is only increased by less than 0.2 dB. Given that $\sigma_\varphi^2(\tau)$ is kept constant (sampled at the system symbol rate), so as the Lorentzian-equivalent linewidth, this 0.2 dB discrepancy represents the inaccuracy of using Lorentzian-equivalent linewidth to estimate system SNR penalty. Similarly, for Fig. 11(b) the FWHM linewidth is increased from 1 MHZ to 6 MHz and 8 MHz for $F_1 = 100$ MHz and $G = 10$ and 20, respectively. The highest discrepancy of system SNR penalty

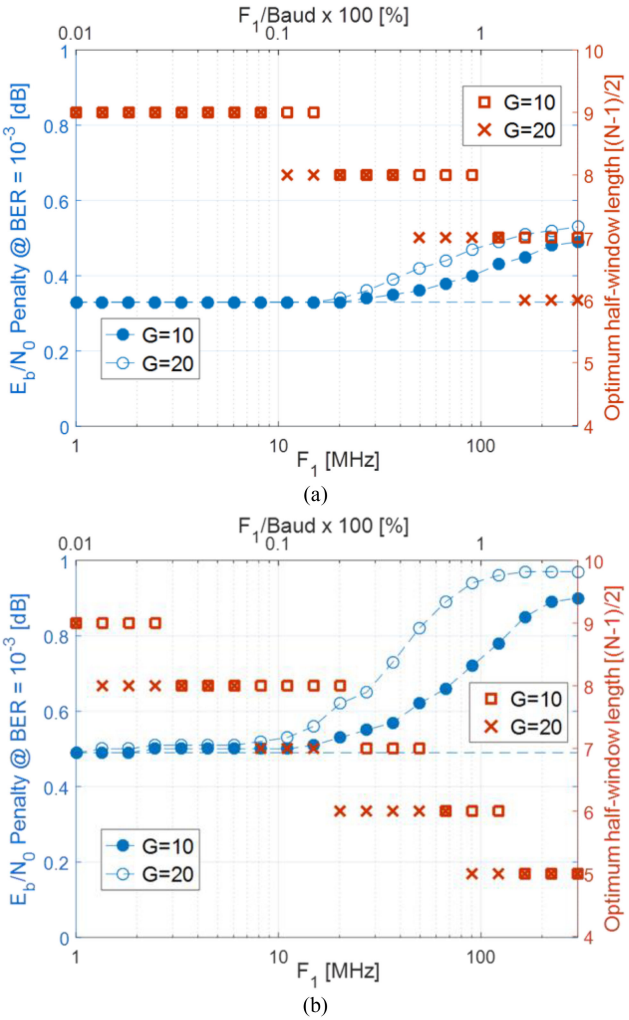

Fig. 11. SNR penalty and optimum window length versus F_1 for differential 16-QAM at 10 GBaud with BPS algorithm and initial ideal Lorentzian laser linewidth of (a) 500 kHz and (b) 1 MHz.

evaluated based on the Lorentzian-equivalent linewidth system is less than 0.45 dB even with a relatively high F_1 of 300 MHz (3% of symbol rate) and an enhancement factor G of 20. This discrepancy is much less than what would be expected based on the FWHM linewidth (e.g., >4 dB for FWHM of 9 MHz, see Fig. 5(a) & (b)), indicating that Lorentzian-equivalent linewidth is a much more accurate parameter to specify the system impact of lasers with non-white FM noise.

V. Conclusion

We have measured phase noise and spectral linewidths of different laser diodes and found that FM noise spectral profiles of these lasers are not always white and can have significant variations at different frequencies for some types of lasers. Excess low-frequency FM noise components may extend up to tens of MHz in some types of lasers, like the QD-MLLs, with more than an order of magnitude ratio compared to higher frequencies. This non-white characteristic of FM noise is found to affect the use of spectral linewidth when estimating the performance of optical systems that require CPR. Based on measured optical phase noise waveforms of different types of lasers, we have shown that the spectral FWHM linewidth alone is not sufficient to characterize phase noise, or to determine its impact on the design of an optimum CPR for coherent receivers for non-white FM noise. Using the measured phase noise from different QD-MLLs with several MHz FWHM linewidths, we have shown by simulation comparable system performance to a DFB laser of only a few hundred kHz FWHM linewidth, due to dissimilarity in their FM noise spectral profiles. This result was further supported by a B2B 16-QAM transmission experiment comparing a QD-MLL with an ECL at a low symbol rate of 5 GBaud. The OSNR penalty was found to be only ~0.7 dB when replacing the ECL (<50 kHz FWHM linewidth) with the QD-MLL (>8 MHz FWHM linewidth) in the experiment, with optimizing the CPR averaging window size. We have also shown that a "Lorentzian-equivalent linewidth", evaluated by sampling the phase noise waveform at a relatively high sampling frequency, can be a reliable and accurate parameter for assessing the impact of laser phase noise in the digital coherent system. The choice of a practical sampling frequency may depend on the characteristics of the phase noise and the SNR in measurement setup. However, we have shown that for a wide practical range of non-white FM noise profiles a sampling frequency at 5 GHz is adequate. Furthermore, by semi-analytical analysis and supporting results from the experimental measurements, the optimum averaging window length in CPR algorithms was shown to be shorter for non-white phase noise with enhanced low-frequency phase noise power spectral density at fixed phase difference variance. This observation suggests that CPR algorithms should be optimized in system design stage based on the actual phase noise data of the laser rather than relying on the ideal Lorentzian model.

Acknowledgment

NRC Canada provided the quantum-dot mode-locked lasers used in this work.

References

[1] E. Agrell *et al.*, "Roadmap of optical communications," *J. Opt.*, vol. 18, no. 6, May 2016, Art. no. 063002.
[2] D. Lavery, S. Erkilinç, P. Bayvel, and R. I. Killey, "Recent progress and outlook for coherent PON," in *Proc. Opt. Fiber Commun. Conf. Expo.*, San Diego, CA, USA, 2018, Paper M3B.1.
[3] M. S. Erkılınç *et al.*, "Comparison of low complexity coherent receivers for UDWDM-PONs (λ-to-the-user)," *J. Lightw. Technol.*, vol. 36, no. 16, pp. 3453–3464, Aug. 15, 2018.
[4] J. Cheng, C. Xie, Y. Chen, X. Chen, M. Tang, and S. Fu, "Comparison of coherent and IMDD transceivers for intra datacenter optical interconnects," in *Proc. Opt. Fiber Commun. Conf.*, 2019, Paper W1F.2.
[5] E. Ip and J. M. Kahn, "Feedforward carrier recovery for coherent optical communications," *J. Lightw. Technol.*, vol. 25, no. 9, pp. 2675–2692, Sep. 2007.
[6] T. Pfau, S. Hoffmann, and R. Noe, "Hardware-efficient coherent digital receiver concept with feedforward carrier recovery for M -QAM constellations," *J. Lightw. Technol.*, vol. 27, no. 8, pp. 989–999, Apr. 15, 2009.
[7] K. Kikuchi, "Fundamentals of coherent optical fiber communications," *J. Lightw. Technol.*, vol. 34, no. 1, pp. 157–179, Jan. 1, 2016.
[8] M. Seimetz, "Laser linewidth limitations for optical systems with high-order modulation employing feed forward digital carrier phase estimation," in *Proc. Conf. Opt. Fiber Commun./Nat. Fiber Opt. Engineers Conf.*, San Diego, CA, USA, 2008, Paper OTuM2.

[9] M. G. Taylor, "Phase estimation methods for optical coherent detection using digital signal processing," *J. Lightw. Technol.*, vol. 27, no. 7, pp. 901–914, Apr. 1, 2009.
[10] I. Fatadin, D. Ives, and S. J. Savory, "Carrier phase recovery for 16-QAM using QPSK partitioning and sliding window averaging," *IEEE Photon. Technol. Lett.*, vol. 26, no. 9, pp. 854–857, May 1, 2014.
[11] X. Zhou, "An improved feed-forward carrier recovery algorithm for coherent receivers with *M*-QAM modulation format," *IEEE Photon. Technol. Lett.*, vol. 22, no. 14, pp. 1051–1053, Jul. 15, 2010.
[12] X. Li, Y. Cao, S. Yu, W. Gu, and Y. Ji, "A simplified feedforward carrier recovery algorithm for coherent optical QAM system," *J. Lightw. Technol.*, vol. 29, no. 5, pp. 801–807, Mar. 1, 2011.
[13] J. Li, L. Li, Z. Tao, T. Hoshida, and J. C. Rasmussen, "Laser-linewidth-tolerant feed-forward carrier phase estimator with reduced complexity for QAM," *J. Lightw. Technol.*, vol. 29, no. 16, pp. 2358–2364, Aug. 15, 2011.
[14] M. Magarini *et al.*, "Pilot-symbols-aided carrier-phase recovery for 100-G PM-QPSK digital coherent receivers," *IEEE Photon. Technol. Lett.*, vol. 24, no. 9, pp. 739–741, May 1, 2012.
[15] S. M. Bilal, C. R. S. Fludger, and G. Bosco, "Multi-stage CPE algorithms for 64-QAM constellations," in *Proc. Opt. Fiber Commun.*, San Francisco, CA, USA, 2014, Paper M2A.8.
[16] S. M. Bilal, G. Bosco, J. Cheng, A. P. T. Lau, and C. Lu, "Carrier phase estimation through the rotation algorithm for 64-QAM optical systems," *J. Lightw. Technol.*, vol. 33, no. 9, pp. 1766–1773, May 1, 2015.
[17] K. Kikuchi, "Characterization of semiconductor-laser phase noise and estimation of bit-error rate performance with low-speed offline digital coherent receivers," *Opt. Exp.*, vol. 20, no. 5, pp. 5291–5302, Feb. 2012.
[18] T. Okoshi, K. Kikuchi, and A. Nakayama, "Novel method for high resolution measurement of laser output spectrum," *Electron. Lett.*, vol. 16, no. 16, pp. 630–631, Jul. 1980.
[19] T. Duthel, G. Clarici, C. R. S. Fludger, J. C. Geyer, C. Schulien, and S. Wiese, "Laser linewidth estimation by means of coherent detection," *IEEE Photon. Technol. Lett.*, vol. 21, no. 20, pp. 1568–1570, Oct. 2009.
[20] M. Al-Qadi, G. Vedala, and R. Hui, "Performance of lasers with excess low-frequency FM-noise profiles in digital coherent optical systems," in *Proc. Opt. Fiber Commun. Conf.*, 2019, Paper W4B.3.
[21] G. Vedala, M. Al-Qadi, M. O'Sullivan, J. Cartledge, and R. Hui, "Phase noise characterization of a QD-based diode laser frequency comb," *Opt. Exp.*, vol. 25, no. 14, pp. 15890–15904, Jun. 2017.
[22] M. Al-Qadi, G. Vedala, and R. Hui, "Phase noise of diode laser frequency comb and its impact in coherent communication systems," in *Proc. Conf. Lasers Electro-Opt.*, May 2018, Paper JTu2A.35.
[23] T. N. Huynh, S. P. Ó. Dúill, L. Nguyen, L. A. Rusch, and L. P. Barry, "Simple analytical model for low-frequency frequency-modulation noise of monolithic tunable lasers," *Appl. Opt.*, vol. 53, no. 5, pp. 830–835, 2014.
[24] T. N. Huynh, L. Nguyen, and L. P. Barry, "Phase noise characterization of SGDBR lasers using phase modulation detection method with delayed self-heterodyne measurements," *J. Lightw. Technol.*, vol. 31, no. 8, pp. 1300–1308, Apr. 2013.
[25] M. Al-Qadi, M. O'Sullivan, C. Xie, and R. Hui, "Differential phase noise properties in QD-MLL and its performance in coherent transmission systems," in *Proc. Conf. Lasers Electro-Opt.*, San Jose, CA, USA, May 2019, Paper SW3O.2.
[26] G. D. Domenico, S. Schilt, and P. Thomann, "Simple approach to the relation between laser frequency noise and laser line shape," *Appl. Opt.*, vol. 49, no. 25, pp. 4801–4807, Sep. 2010.
[27] N. Bucalovic *et al.*, "Experimental validation of a simple approximation to determine the linewidth of a laser from its frequency noise spectrum," *Appl. Opt.*, vol. 51, pp. 4582–4588, 2012.
[28] Q. Zhou *et al.*, "Power-area method to precisely estimate laser linewidth from its frequency-noise spectrum," *Appl. Opt.*, vol. 54, pp. 8282–8289, 2015.
[29] R. Hui and M. O'Sullivan, "Characterization of optical devices," in *Proc. Fiber Opt. Meas. Techn.*, Burlington, MA, USA: Academic, 2009, pp. 259–276.
[30] R. Maher and B. Thomsen, "Dynamic linewidth measurement technique using digital intradyne coherent receivers," *Opt. Exp.*, vol. 19, no. 26, pp. B313–B322, Dec. 2011.
[31] Z. G. Lu, J. R. Liu, S. Raymond, P. J. Poole, P. J. Barrios, and D. Poitras, "312-fs pulse generation from a passive C-band InAs/InP quantum dot mode-locked laser," *Opt. Exp.*, vol. 16, no. 14, pp. 10835–10840, Jul. 2008.
[32] A. Moscoso-Mártir *et al.*, "8-channel WDM silicon photonics transceiver with SOA and semiconductor mode-locked laser," *Opt. Exp.*, vol. 26, no. 19, pp. 25446–25459, Sep. 2018.
[33] J. N. Kemal *et al.*, "32QAM WDM transmission using a quantum-dash passively mode-locked laser with resonant feedback," in *Proc. Opt. Fiber Commun. Conf. Exhib.*, Los Angeles, CA, USA, 2017, Paper TH5C.3.
[34] N. Eiselt *et al.*, "Real-time 200 Gb/s (4 × 56.25 Gb/s) PAM-4 transmission over 80 km SSMF using quantum-dot laser and silicon ring-modulator," in *Proc. Opt. Fiber Commun. Conf.*, 2017, Paper W4D.3.
[35] J. N. Kemal *et al.*, "WDM transmission using quantum-dash mode-locked laser diodes as multi-wavelength source and local oscillator," in *Proc. Opt. Fiber Commun. Conf. Exhib.*, Los Angeles, CA, USA, 2017, Paper Th3F.6.
[36] M. Al-Qadi, G. Vedala, M. O'Sullivan, C. Xie, and R. Hui, "QD-MLL-based single-sideband superchannel generation scheme with Kramers–Kronig direct detection receivers," *IEEE Photon. J.*, vol. 11, no. 4, pp. 1–13, Aug. 2019.
[37] K. S. Shanmugan and A. M. Breipohl, *Random Signals: Detection, Estimation and Data Analysis*. New York, NY, USA: Wiley, 1988.
[38] H. Cramér, *Mathematical Methods of Statistics*. Princeton, NJ, USA: Princeton Univ. Press, Mar. 23, 1999.
[39] F. Rice, B. Cowley, B. Moran, and M. Rice, "Cramér-Rao lower bounds for QAM phase and frequency estimation," *IEEE Trans. Commun.*, vol. 49, no. 9, pp. 1582–1591, Sep. 2001.